Structural Performance Evaluation of Hybrid Damping Device Combining Steel Slit with Vulcanized Rubber

Joon-Ho Lee [1,*] and Yu-Seong Kim [2]
[1] Department. of Architectural Engineering, Seoul University, Seoul, Republic of Korea
[2] Plus Structural Engineering Inc., Seoul, Republic of Korea
Email: joonho.lee.97@gmail.com (J.H.L.); batman0961@gmail.com (Y.S.K.)
*Corresponding author

***Abstract*—It is efficient to construct a device by combining two or more damping devices to respond to various vibration sources, and diverse type of damping devices are being developed recently. In this study, HSR hybrid damper (Hybrid Slit damper with vulcanized Rubber) in which vulcanized rubber and steel slit plate are combined in parallel was proposed and experiments were performed to analyze the seismic performance. Vulcanized rubber dissipates seismic energy through shear deformation and has great initial stiffness. Compared with the conventional slit dampers with the same yield strength, the hybrid damper has an advantage in that only vulcanized rubber is activated for small earthquakes or strong wind, and both vulcanized rubber and slit damper work simultaneously for strong earthquakes. Cyclic loading tests of damper specimens are carried out to evaluate their seismic energy dissipation capability in accordance with criteria presented in KDS 41 17 00 and MOE 2019. In addition, the second-floor full-scale reinforced concrete frame test was performed, and the test results were analyzed. Test result shows that the damping devices installed using the proposed procedure are effective in restraining the building displacement within a given target performance limit state.**

***Keywords*—hybrid damper, hybrid damping device, vulcanized rubber, steel slit damper, seismic performance evaluation**

I. Introduction

It is efficient to construct a device by combining two or more damping devices to respond to various vibration sources, and diverse type of damping devices are being developed recently. In this study, HSR hybrid damper (Hybrid Slit damper with vulcanized Rubber) in which vulcanized rubber and steel slit plate are combined in parallel was proposed and experiments were performed to analyse the seismic performance. Vulcanized rubber dissipates seismic energy through shear deformation and has great initial stiffness. Compared with the conventional slit dampers with the same yield strength, the hybrid damper has an advantage in that only vulcanized rubber is activated for small earthquakes or strong wind, and both vulcanized rubber and slit damper work simultaneously for strong earthquakes. Cyclic loading tests of damper specimens are carried out to evaluate their seismic energy dissipation capability in accordance with criteria presented in KDS 41 17 00 and MOE 2019. In addition, the second-floor full-scale reinforced concrete frame test was performed, and the test results were analyzed. Test result shows that the damping devices installed using the proposed procedure are effective in restraining the building displacement within a given target performance limit state.

II. Proposed Hybrid Steel Slit Damper with Vulcanized Rubber (HSR)

A. Configuration of HSR Damper

The shape of the HSR damper is shown in Fig. 1, it is a composite damping device that dissipates energy when a lateral load is generated by combining high damping rubber in parallel with a slit plate. The high damping rubber is vulcanized and bonded to the steel plate and is combined with the slit plate through the upper and lower plate surfaces. Since the high-damping rubber and the slit plate are combined in parallel, it is possible to have a composite damping effect for various vibration sources through the damping effect caused by the plastic deformation of the steel slit and the shear deformation of the high-damping rubber.

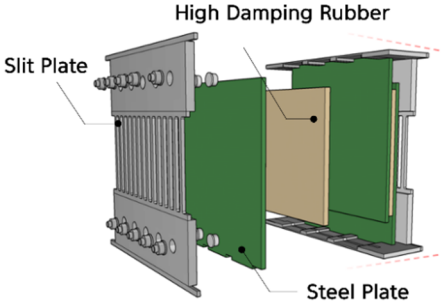

Fig. 1. Configuration of hybrid slit damping device with vulcanized rubber.

Manuscript received February 2, 2024; revised February 21, 2024; accepted March 3, 2024; published September 25, 2024.

The slit plate damper is composed of steel struts that arranges slit holes in the in-plane direction. Before yielding occurs, steel struts increase the stiffness and load capacity of the structure like a structural member, and After yielding, can have a damping effect through in-plane yield deformation of steel sturts. slit plate damper has an advantage in that manufacturing cost is low and easy to design because of stiffness and strength that can be easily adjusted through the thickness of a steel plate or the number of struts. The vulcanized rubber of the HSR damper is a natural rubber-based viscoelastic material with damping performance When shear deformation occurs, it uses the stiffness and viscosity of viscoelastic materials to dissipate seismic energy.

B. Slit Plate Damping Device

Slit plates are steel hysteretic damping devices with slit holes arranged in the in-plane direction. They are composed of multiple steel strips and achieve damping effects via in-plane yield deformation. Before yielding, they reinforce the stiffness and internal force of a structure, similar to other conventional materials, rather than produce damping effects for energy dissipation. These slit plate damping devices are beneficial in that their manufacturing costs are low, and the major design variables, stiffness, and strength can easily be modified by adjusting the thickness of the steel plate or the number of strips. The slit plate used for the HRS damping device is shown in Fig. 2. Eq. (1) gives the stiffness of the slit damper per unit by representing the moment of inertia for one slit surface as $tb^3/12$. Here, E represents the modulus of elasticity of the steel used, I represents the moment of inertia of the slit surface, l_0 represents the length of the slit, c represents the end fixity coefficient of the steel slate (assume $c = 1$), n represents the number of steel slit strips, t represents the thickness of the strip, and b is the width of the strip.

$$k_d = cn\frac{12EI}{{l_0}^3} = cn\frac{Etb^3}{{l_0}^3} \tag{1}$$

When the deformation of the steel slits exceeds the yield displacement due to the lateral force, both ends of the strip yield, the shear face yields, and a plastic moment M_p , as shown in Eq. (2), occurs. Here, σ_y denotes the yield strength of the steel.

$$M_p = \sigma_y \frac{tb^2}{4} \tag{2}$$

If the lateral force P and the displacement δ_p are assumed to be perfectly elastoplastic, the energy conservation law produces Eq. (3). For infinitesimal deformation, the plastic displacement amount δ_p can be $l_0\theta_p$, leading to the yielding load of the slit damping device P_y , as presented in Eq. (4). Moreover, the yield deformation of the slit device can be computed from Eq. (5), based on the relationship between Eq. (1) and Eq. (4).

$$\frac{1}{2}P_y\delta_p = nM_p\theta_p \tag{3}$$

$$P_y = \frac{2nM_p}{l_0} = \frac{n\sigma_y tb^2}{2l_0} \tag{4}$$

$$\delta_y = 0.5\varepsilon_y {l_0}^2/b \tag{5}$$

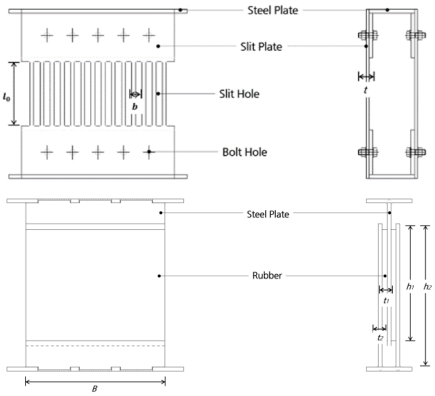

Fig. 2. Shape of slit plate and vulcanized rubber.

C. Theoretical Hysteresis Curve of the High-Damping Rubber and the HRS Damper

The high-damping rubber used in the HRS damping device is a viscoelastic material made from natural rubber. It achieves its damping effects by dissipating seismic energy through the stiffness and viscosity of its viscoelastic material. The shear yield strength was computed from the shear modulus of the high-damping rubber (G') as well as its thickness (t), length (l_0), and shear strain (γ) corresponding to the design displacement (Δ). When arranged in terms of lateral deformation, the shear yield strength can be expressed as follows.

$$V = 2G't_1\Delta \tag{6}$$

The theoretical hysteresis curve of the HRS damper can be predicted from the sum of the physical properties of each damping element because the slit-plate damping devices and high-damping rubber are combined in parallel. The initial stiffness of the HRS damper (K_{Hybrid}) can be represented by the sum of the slit-plate stiffness (K_{slit}) and the high-banding rubber stiffness, (K_{Rubber}) as given in Eq. (7). The yield strength can be computed by adding Eq. (8) and Eq. (9), as can the yield displacement. Therefore, it can be visualized as a bilinear or a trilinear curve.

$$K_{Hybrid} = K_{slit} + K_{Rubber} \tag{7}$$

$$F_{y1} = F_{y,S} + K_{Rubber}D_s \tag{8}$$

$$F_{y2} = F_{s,R} + F_{y,R} \tag{9}$$

III. Structural Performance Test of HSR Damper

For the structural performance test of the HSR damper, the standard required performance was analyzed by performing a cyclic loading test according to the seismic building design code of the Korean design standard (KDS 41 17 00)[9] and Seismic performance evaluation and reinforcement manual in Korea (MOE 2019)[10] (see in Fig. 3).

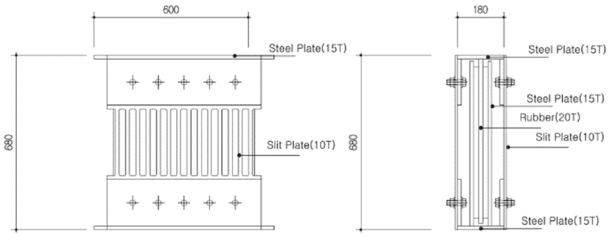

Fig. 3. Shape of HRS damper specimen.

A. Plan of Specimen

Specimen of the HSR damping device was manufactured by vulcanizing and bonding high damping rubber to the slit plate of SS275(Fy=275Mpa) shown in Fig. 2. 1000kN hydraulic sub-actuator apply load repeatedly in the horizontal direction, and the displacement was confirmed by installing a Linear Variable Differential Transformer (LVDT) to measure the displacement of the specimen. Cyclic loading test setup was shown in Fig. 4.

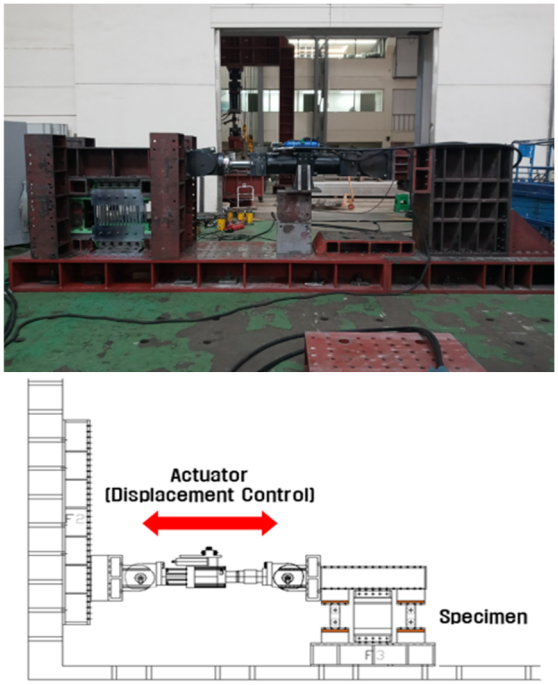

Fig. 4. Cyclic loading test setup.

B. Load Protocol and Standard Required Performance

KDS 41 17 00 and MOE 2021 suggest a standard loading protocol to analyze whether or not the standard required performance is satisfied after cyclic loading tests. The loading protocol for each loading test is shown in Fig. 5. The load protocol of the Cyclic loading test (KDS 41 17 00) was conducted by setting 0.33 times the target displacement (Δ_m) 10 times, 0.67 times 5 times, and 1.0 times 3 times, and the load protocol of the cyclic loading test(MOE 2019) was conducted by setting 0.25 times of the target displacement(Δ_m) 10 times, 0.5 times 5 times, and 1.0 times 3 times.

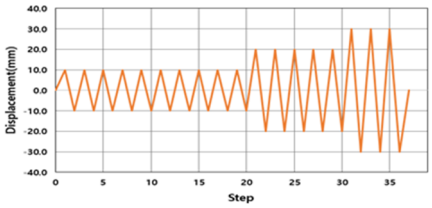

(a) KDS 41 17 00

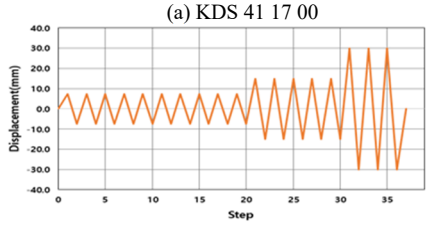

(b) MOE 2021

Fig. 5. Load protocol for cyclic loading test.

C. Results of Structural Performance Test

Fig. 6 is a graph showing the load-displacement curve according to the results of cyclic loading tests (KDS 41 17 00, MOE 2021). The maximum strength of the test specimen was 422.19kN in the case of the repeated load test (KDS 41 17 00), and the test specimen in the cyclic loading test (MOE 2021) was 402.97kN. Stable hysteretic behavior was exhibited without deterioration of strength for each cycle. At the loading stage ($0.33\Delta_{m(KDS)}$, $0.25\Delta_{m(MOE)}$) at the yield deformation point of the steel strut, the energy dissipation area appeared wide in the transverse direction, like the hysteretic characteristics due to the plastic deformation of the steel slit. From the subsequent loading stage, As the shear strain of high damping rubber increases, the energy dissipation area gradually increases in the longitudinal direction due to the effect of the hyperelastic behavior of the high damping rubber. It is believed that the hysteresis characteristics of the steel slit dominate at low displacement, and the hysteresis characteristics of the high-damping rubber dominate after the yield deformation of the steel slit.

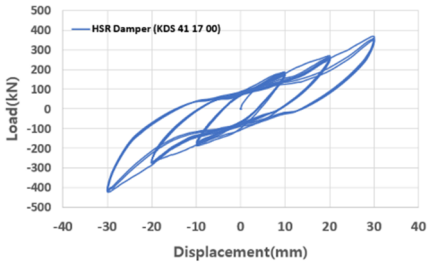

(a) KDS 41 17 00

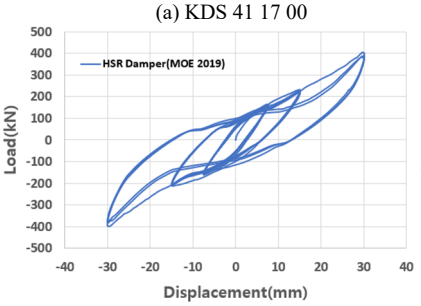

(b) MOE 2021

Fig. 6. Load-displacement curve.

IV. Loading Test of RC Frame

A. Specimen Plan and Method

In order to compare the seismic performance of frames reinforced with HSR dampers, non-reinforced frames (RCF-N), internal reinforced frames (RCF-Q-I), and externally reinforced frames (RCF-Q-E) were manufactured and tested (see in Fig. 7).

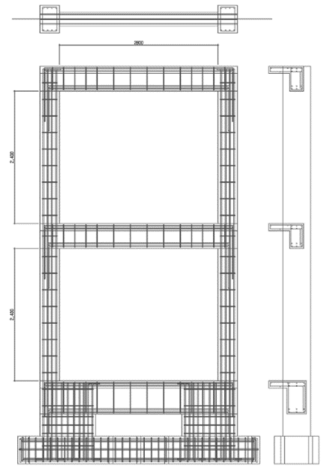

(a) RCF-N Specimen

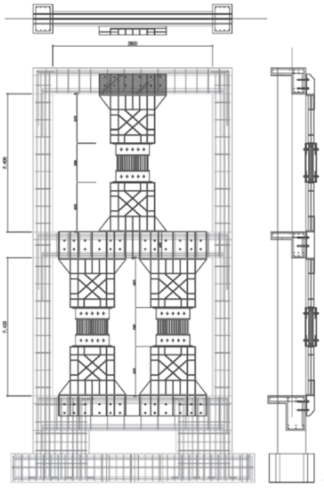

(b) RCF-Q-E Specimen

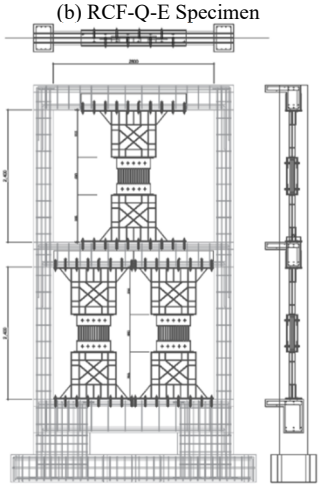

(c) RCF-Q-I specimens

Fig. 7. RC frame specimen and reinforced frame specimens strengthened by HSR damper.

The RCF-N frame was manufactured as a two-story RC frame with a size similar to the real RC Structure. it was designed as a column shear failure type based on previous data on non-seismic designed RC buildings. In the case of reinforced frame, the existing RC frame is the same, and the HRS damper was reinforced by combining to the upper and lower plates of the connecting frame. The load protocol is based on 'FEMA-461, Interim Testing Protocol for Determining the Seismic Performance Characteristics of Structural and Nonstructural Components' [11]. It was that the minimum displacement (Δ_0) was assumed to be 3.04mm based on story drift of the two-story beam, and 1.4 times for each cycle. By amplifying the displacement shown in Fig. 8, an incremental loading test was performed until the strength of the specimen was sufficiently reduced.

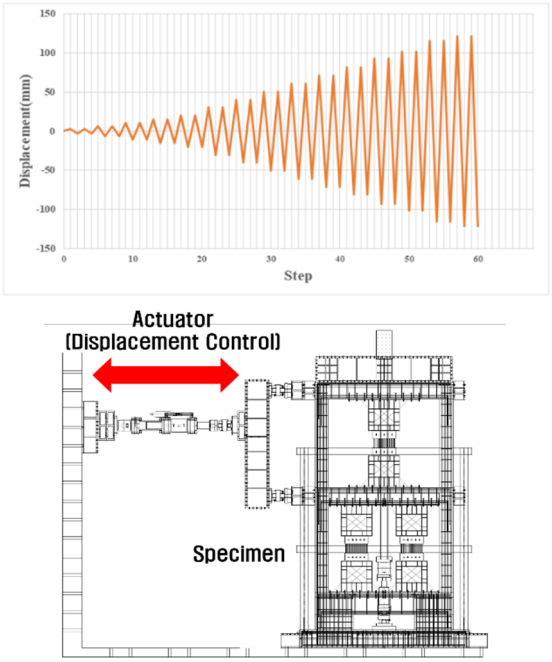

Fig. 8. Load protocol and loading test setup.

B. Result of RC Frame Test

The load-displacement curve as a result of the RC frame test is shown in Fig. 9. In the case of the RCF-N specimen, the maximum strength was 108.54 kN at an additional load of 2.15% of the story drift ratio, and stable hysteretic behavior was exhibited without loss of strength to 13 steps at the CP level (2.1%). As for final failure pattern, shear failure occurred at the lower part of the column on the first floor and the beam-column joint due to the diagonal crack at the story drift ratio of 0.65%.

In the case of the RCF-Q-E specimen, the maximum strength was 176.59 kN at an additional load at story drift ratio of 1.53%, and stable hysteretic behavior was shown without strength to 13 steps corresponding to the CP level (2.1%). As for the final failure pattern, initial bending cracks occurred at the lower part of the column on the first floor at story drift ratio of 0.2%, and shear cracks began to occur at the lower portion of the column on the first floor at an interlayer displacement ratio of 0.8%. In contrast to the RCF-N specimen, cracks did not increase significantly.

In the case of the RCF-Q-I specimen, the maximum strength was 254.95 kN at story drift ratio of 2.18%, and stable hysteretic behavior was exhibited without loss of strength to 13 steps corresponding to the CP level (2.1%). As for the final failure pattern, initial bending cracks occurred at the lower part of the column on the first floor at story drift ratio of 0.25%, and shear cracks began to occur at the lower portion of the column on the first floor at an story drift ratio of 0.8%. In contrast to the RCF-N specimen, cracks did not increase significantly.

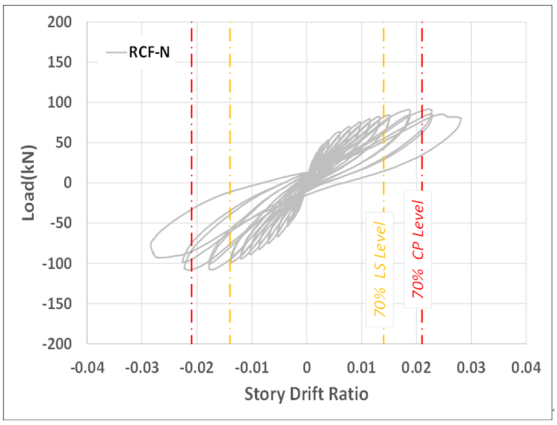

(a) RCF-N specimen

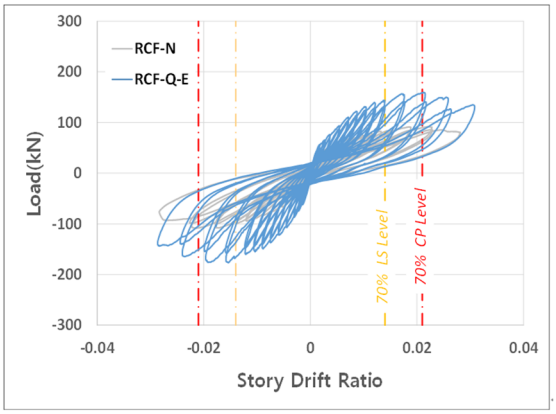

(b) RCF-Q-E specimen

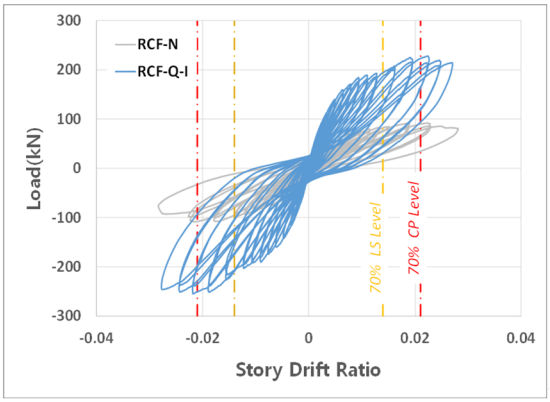

(c) RCF-Q-I speecimen

Fig. 9. Load-displacement curve.

Fig. 10 is a graph showing the capacity of energy dissipation of each specimen. In the RCF-N specimen, the energy dissipation began to increase rapidly at the lateral displacement ratio of 1.4%, where the first crack occurred in the beam-column connection, and the cumulative energy dissipation amount was 17590.1 kN·mm until the final loading step. The Cumulative energy dissipation of RCF-Q-E and RCF-Q-I Specimens was 44922.04 kN mm and 41975.12 kN mm, respectively, until the final loading step. Compared to the RCF-N specimen, the capacity of energy dissipation of reinforced specimen increased, and the cumulative energy dissipation of the RCF-Q-I specimen was 1.07 times higher than that of the RCF-Q-E specimen.

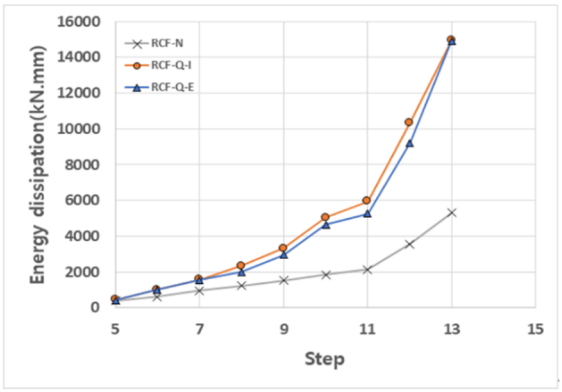

(a) Energy dissipation capacity

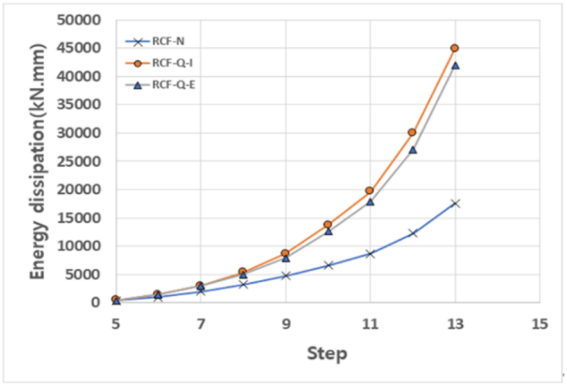

(b) Cumulative energy dissipation capacity

Fig. 10. Energy dissipation capacity.

V. Conclusion

In this study, a hybrid damping device combining high-damping rubber and a slit plate was proposed, and structural performance tests and RC frame tests were conducted to analyze seismic performance. The results are as follows.

(1) As a result of the cyclic loading test, the maximum and minimum load for each cycle, maximum and minimum load at zero displacement, and energy dissipation were within 15% of the average value for each cycle, satisfying the standard required performance of KDS 41 17 00 and MOE 2021.

(2) As a result of the analysis of hysteresis characteristics, hysteresis characteristics due to plastic deformation of steel slits were dominant at low displacement, and after yield deformation of steel slit hysteresis characteristics of high-damping rubber due to shear deformation were dominant.

(3) As a result of the RC frame test, the unreinforced test specimen (RCF-N), the internally fitted reinforced specimen (RCF-Q-I), and the externally attached reinforced specimen (RCF-Q-E) all satisfied the permissible story drift ratio according to seismic performance level
(4) Compared to the RCF-N Specimen, the energy dissipation of the reinforced specimens(RCF-Q-E, RCF-Q-I) increased, and the cumulative energy dissipation of the internally fitted reinforced specimen(RCF-Q-I) increased the most by 2.55 times.

CONFLICT OF INTEREST

The authors declare no conflict of interest.

AUTHOR CONTRIBUTIONS

All authors performed the experiment; Lee contributed to the analysis of experimental data and the writing of the paper; Kim contributed to finishing the paper; all authors had approved the final version.

FUNDING

This work has supported by the National Research Foundation of Korea (NRF) grant funded by the Korea government (MSIT)(No.2020R1C1C1005779).

REFERENCES

[1] J. E. Roh and S. H. Lee, "Experimental evaluation of a multi-action hybrid damper under cyclic loading," *Journal of the Architectural Institute of Korea Structure & Construction*, vol. 32, pp. 3–9, 2016, doi:10.5659/JAIK_SC.2016.32.11.3J.
[2] D. H. Kim, "Development of hybrid damper systems for the vibration control of wind and earthquake," *The Magazine of the Korean Society for Advanced Composite Structures*, vol. 11, pp. 18–19, 2020
[3] W. S. Pong, C. S. Tsai, and G. C. Lee, *Seismic Performance of High-Rise Building Frames with Added Energy-absorbing Devices* (NCEER-94-0016), Natianal Center for Earthquake Engineering Research, Red Jacket Quadrangle, Buffalo, NY, 1994.
[4] K. Uetani, M. Tsuji, and I. Takewaki, "Application of an optimum design method to practical building frames with viscous dampers and hysteretic dampers," *Eng. Struct.,* vol. 25, no. 5, pp. 579–592, 2003, http://dx.doi.org/10.1016/S0141-0296(02)00168-2.
[5] J. D. Marshall and F. A. Charney, "Seismic response of steel frame structures with hybrid passive control systems," *Earthq. Eng. Struct. Dyn.*, vol. 41, no. 4, pp. 715–733, 2012, http://dx.doi.org/10.1002/eqe.1153.
[6] Y. Murakami, K. Noshi, K. Fujita, M. Tsuji, and I. Takewaki, "Simultaneous optimal damper placement using oil, hysteretic and inertial mass dampers," *Earthq. Struct.* vol. 5, no. 3, pp. 261–276, 2013, http://dx.doi.org/10.12989/eas.2013.5.3.261.
[7] J. Lee and J. Kim, "Seismic performance evaluation of moment frames with slit-friction hybrid dampers," *Earthq. Struct.*, vol. 9, no. 6, pp. 1291–1311, 2015
[8] K. Uetani, M. Tsuji, and I. Takewaki, "Application of an optimum design method to practical building frames with viscous dampers and hysteretic dampers," *Eng. Struct.*, vol. 25, no. 5, pp. 579–592, 2003, http://dx.doi.org/10.1016/S0141-0296(02)00168-2.
[9] J. Kim and H. Shin, "Seismic loss assessment of a structure retrofitted with slit-friction hybrid dampers," *Eng. Struct.*. vol. 130, 2017, pp. 336–350
[10] FEMA, "Interim testing protocols for determining the seismic performance characteristics of structural and nonstructural components (FEMA-461)," pp. 21–23, 2007.
[11] Architectural Institute of Korea, "Seismic building design code and commentary: KDS 41 17 00," pp. 136–139, 2019.
[12] Ministry of Education, "Seismic performance evaluation and reinforcement manual for school facilities," p. 97, 2021.